Yield Criteria and Strain-Rate Behavior of $Zr_{57.4}Cu_{16.4}Ni_{8.2}Ta_8Al_{10}$ Metallic-Glass-Matrix Composites

R.T. OTT, F. SANSOZ, T. JIAO, D. WARNER, C. FAN, J.F. MOLINARI, K.T. RAMESH, and T.C. HUFNAGEL

We have examined the yielding and fracture behavior of $Zr_{57.4}Cu_{16.4}Ni_{8.2}Ta_8Al_{10}$ metallic-glass-matrix composites with a small volume fraction (~4 pct) of ductile crystalline particles under quasi-static uniaxial tension and compression and dynamic uniaxial compression. The yield stress of the composite is the same for quasi-static tension and compression, consistent with a von Mises yield criterion. The measured average angle between the shear bands and the loading axis in quasi-static compression is 47 ± 2 deg, significantly larger than the value of ~42 deg typically reported for single-phase metallic glasses. Finite element modeling (FEM) shows that the measured value is consistent with both the von Mises criterion (48 ± 4 deg) and the Mohr–Coulomb criterion (46 ± 5 deg). The fracture surface angles, however, are 41 ± 1 deg (compression) and 54 ± 2 deg (tension), in good agreement with observations of single-phase metallic glasses. At low strain rates ($<10^{-1}$ s^{-1}), the yield stress is independent of strain rate, while at higher strain rates ($>10^{0}$ s^{-1}), the failure stress decreases with increasing strain rate, which again is similar to the behavior of single-phase glasses. These results indicate that while the presence of the particles has a significant effect on the yield behavior of the composites, the fracture behavior is largely governed by the properties and behavior of the amorphous matrix.

I. INTRODUCTION

YIELD criteria are important for predicting the behavior of ductile engineering materials under multiaxial loading conditions and can also provide insight into underlying mechanisms of deformation. The question of which yield criterion is most appropriate for metallic glasses has received considerable attention in the literature. Two popular choices have been the von Mises criterion:

$$k = \frac{\sqrt{6}}{6}\left[(\sigma_1 - \sigma_2)^2 + (\sigma_2 - \sigma_3)^2 + (\sigma_1 - \sigma_3)^2\right]^{1/2} \quad [1]$$

where k is the yield stress in pure shear and $\sigma_1 \geq \sigma_2 \geq \sigma_3$ are the principal stresses and the Mohr–Coulomb criterion:

$$k = \tau + \alpha\sigma_n \quad [2]$$

where τ and σ_n are the shear stress and the normal stress on the slip plane, respectively, and α is a constant. Some of the early work on Pd-based glasses[1] suggested that the von Mises criterion was most appropriate, while other researchers favored the Mohr–Coulomb criterion.[2]

The development of new Zr-based alloys with outstanding glass-forming ability in the early 1990s created new interest in the properties of metallic glasses and facilitated studies of mechanical behavior by providing bulk specimens for testing. The most obvious difference between the von Mises and Mohr–Coulomb criteria is that the former predicts that the yield stress will be the same in uniaxial tension and compression, while the latter predicts that they will be different. Reports in the literature differ on this point. Zhang and co-workers, for instance, report that the yield stress is significantly lower in tension than in compression,[3] while Lewandowski and co-workers report no significant difference.[4] Complicating matters is the fact that what is usually reported is a *fracture* stress, not a yield stress. Because metallic glasses do not strain harden, they are susceptible to shear localization and premature fracture initiating at defects. Thus, it is not clear that any tension/compression asymmetry reported solely on the basis of fracture stresses actually represents the fundamental yielding behavior of the material.

Other studies, however, also favor the Mohr–Coulomb criterion. For instance, indentation studies and FEM on metallic glasses show that the load-displacement curves appear to show pressure- or normal-stress dependence.[5,6] Furthermore, Schuh and Lund[7,8,9] have used atomistic simulations to model yielding in metallic glasses; they also report that the yield stresses exhibited by metallic glasses can be described in the framework of the Mohr–Coulomb criterion. The predicted value of $\alpha = 0.123$ for their simulations was found to compare well with the experimentally determined values of 0.11 to 0.13.[2,5]

Several authors have also used fracture surface angles to infer the underlying yield behavior of metallic glasses. Again, the assumption (sometimes implicit) is that the fracture occurs on the same planes as slip. Under the von Mises

R.T. OTT, Postdoctoral Fellow, is with the Materials and Engineering Physics Program, Ames Laboratory (USDOE), Ames, IA 50011. Contact e-mail: rtott@ameslab.gov F. SANSOZ, Assistant Professor, is with the School of Engineering, University of Vermont, Burlington, VT 05405. T. JIAO, formerly Postdoctoral Fellow, Department of Mechanical Engineering, Johns Hopkins University, Baltimore, MD 21218, is Postdoctoral Research Associate, Division of Engineering, Brown University, Providence, RI 02912. D. WARNER, Graduate Student, and J.F. MOLINARI and K.T. RAMESH, Professors, Department of Mechanical Engineering, and T.C. HUFNAGEL, Professor, Department of Materials Science and Engineering, are with Johns Hopkins University. C. FAN, formerly Postdoctoral Fellow, Department of Materials Science and Engineering, Johns Hopkins University, is Research Assistant Professor, Department of Materials Science and Engineering, University of Tennessee, Knoxville, TN 37996.

Manuscript submitted March 6, 2006.

criterion, yielding in uniaxial loading occurs on the plane of maximum shear stress (45 deg to the loading axis), while under the Mohr–Coulomb criterion, the fracture surface will deviate from 45 deg, being smaller for compression and larger for tension. A summary of some available data is presented in Table I. Generally speaking, the more recent data tend to support a tension/compression asymmetry in both the flow stress and the fracture or slip plane angle. A complication is that the unmodified Mohr–Coulomb criterion would predict a symmetric deviation of 45 deg $\pm \theta$, while in reality an asymmetric deviation is usually observed. Zhang and Eckert have presented a modified Mohr–Coulomb criterion to account for this.[10]

The deformation behavior of metallic-glass-matrix composites has been less studied. Deformation of metallic glass composites is more complicated because it is often dependent on dislocation motion in the reinforcing phase (if it is ductile) and shear banding in the glass matrix. Furthermore, the presence of a reinforcing phase affects shear band initiation and propagation in the glass matrix. Szuecs and co-workers[11] and Lee and co-workers[12] both reported a tension/compression yield stress asymmetry for ductile dendritic reinforced metallic glass. Lee and co-workers[12] found that the magnitude of the asymmetry between the yield stresses decreased with increasing volume fraction of second-phase dendrites. Additionally, for particle-reinforced composites, the average angle between the shear bands and the compressive loading axis (~43 deg) is consistent with the Mohr–Coulomb criterion.[13] Therefore, the reported yield behavior of several metallic-glass-matrix composites appears to be similar to that of monolithic metallic glasses.

In this article, we report on the deformation behavior of an *in-situ* formed Zr-based composite containing a small volume fraction (~4 pct) of micron-scale Ta-rich particles dispersed in an amorphous matrix. We observe no difference between the yield stresses in quasi-static tension and quasi-static compression. Furthermore, for quasi-static compression, the measured shear band angle is greater than 45 deg, in contrast to single-phase glasses where it is less than 45 deg. On the other hand, the angles between the *fracture* surfaces and the loading axis are consistent with reports for single-phase glasses. Furthermore, the strain-rate dependence of the yield stress (at low strain rates) and the fracture stress (at high strain rates) is similar to that of monolithic metallic glasses. Taken together, our observations indicate that while the presence of the particles can have a significant effect on the yielding behavior of the composites, the fracture behavior is still governed by the behavior of the amorphous matrix.

II. EXPERIMENTAL AND NUMERICAL APPROACH

A. *Sample Preparation and Mechanical Testing*

Composite alloys of composition $Zr_{57.4}Cu_{16.4}Ni_{8.2}Ta_8Al_{10}$ were prepared by arc melting high-purity elements under an Ar environment. The microstructure of the resulting alloys consists of about 4 vol pct bcc Ta-rich particles in an amorphous matrix. Details of the two-step process used to synthesize the alloys is described in detail elsewhere.[14] The alloys were suction cast into a copper mold to form rods ~3 mm in diameter. The samples were machined to rods and rectangular prisms with an aspect ratio of 2:1 for the uniaxial compression tests and 0.6:1 for the Kolsky-bar testing. The ends of the samples were polished to ensure parallelism during the tests.

Samples were loaded in uniaxial compression in an MTS servohydraulic testing machine at strain rates from 10^{-4} to 10^{-0} s^{-1}. The sample strain during compression was calculated by measuring the overall displacement between the two platens using a linear voltage displacement transducer (LVDT). To prevent barreling of the samples during testing, lubricant was applied to the sample ends to reduce the friction between the samples and the platens.

Dynamic tests with strain rates between 10^3 and 10^4 s^{-1} were performed on a compression Kolsky bar. To avoid

Table I. Measured Flow Stresses and Fracture or Slip Plane Angles for Metallic Glass Alloys Loaded in Uniaxial Tension and Uniaxial Compression

	Uniaxial Tension		Uniaxial Compression		
Composition	Flow Stress, σ_f (MPa)	Fracture or Slip Plane Angle (Deg)	Flow Stress, σ_f (MPa)	Fracture or Slip Plane Angle (Deg)	Reference
$Pd_{80}Si_{20}$	1330	90	—	—	35
$Pd_{82}Si_{18}$	2700	45	—	—	36
$Pd_{80}Cu_{20}$	1240	55	—	—	37
$Pd_{80}Au_4Si_{16}$	2700	45	—	—	36
$Pd_{77.5}Cu_6Si_{16.5}$	1500	51	—	—	38
$Pd_{78}Cu_6Si_{16}$	1450	55	—	—	39
$Pd_{40}Ni_{40}P_{20}$	—	—	1750 ± 50	41.9 ± 1.2	40
$Pd_{40}Ni_{40}P_{20}$	~1700	56	—	—	23
$Ni_{76}P_{16}C_4Si_2Al_2$	2000	45	—	—	41
$Zr_{55}Ni_5Cu_{30}Al_{10}$	1310	53 to 60	—	—	25
$Zr_{63}Ni_9Cu_{18}Al_{10}$	—	—	1700	40	22
$Zr_{52.5}Ti_5Ni_{14.6}Cu_{17.9}Al_{10}$	1650	54	1865	45	25
$Zr_{52.5}Ti_5Ni_{14.6}Cu_{17.9}Al_{10}$	1660 ± 420	55 to 65	1820 ± 130	40 to 45	20
$Zr_{40}Ti_{14}Ni_{10}Cu_{12}Be_{24}$	—	—	1900	42	21
$Zr_{40.1}Ti_{12}Ni_{9.3}Cu_{12.2}Be_{26.4}$	1980 ± 20	51.6 ± 1.5	2000 ± 70	40.8 ± 1.4	4
$Zr_{59}Ti_3Ni_8Cu_{20}Al_{10}$	1580 ± 20	54	1690 ± 20	43	3,24

plastic deformation of the bars (and retain appropriate end conditions), we used WC-Co plates (96 pct WC) as compression platens. The ends of the specimen were lubricated with lithium grease to minimize friction. We used copper pulse shapers between the impacting projectile and the incident bar to achieve an equilibrated state of stress and develop a uniform strain state in the specimen up to the point of failure. Additional details of the Kolsky bar technique may be found elsewhere.[15]

B. *Finite Element Modeling*

We also examined the deformation of the composite alloys using FEM to construct a two-dimensional (2-D) plane-strain computational model. We have previously found that this model accurately reproduces both the elastic and plastic behavior (particularly the onset of plasticity) of the composite alloys.[16] The calculations were conducted by assigning a series of compressive displacement increments to the top section of the mesh, while constraining the bottom nodes in the direction of loading. To obtain a representative model of the composite microstructure, a mosaic image was created from micrographs of different regions of the microstructure. Figure 1 shows the mosaic image of the composite microstructure along with the corresponding mesh, which was created using the ppm2oof software.[17]

For the FEM calculations, the constitutive properties of pure polycrystalline Ta were used and the glass matrix was assumed to be elastic-perfectly plastic with no work hardening (Table II). In what follows, we are explicitly not trying to model shear banding in the glass. Instead, we are interested in the stress state in the glass, which is nonuniform due to the effect of the particles. We assume that if the macroscopic yield criterion is satisfied locally, the glass will yield and that the path of the shear bands, at least initially, will be to follow regions where the macroscopic yield criterion (either von Mises or Mohr–Coulomb) is attained. The average value of each component of the 2-D stress tensor over the glass matrix is defined by the average value of the corresponding stress components over the quadrature points of all the matrix elements. The von Mises effective stress in the alloy was calculated on the basis of these average values of stress. The Mohr–Coulomb stress at each quadrature point was calculated using Eq. [2] using a value α of 0.112, which is consistent with experimentally determined values.[2,5] The Mohr–Coulomb stress

Table II. Constitutive Properties of Ta Particles and Glass Matrix for FEM Calculations

Material	σ_y (MPa)	E (GPa)	ν	ε_0^p	n
Ta particles	350	185[42]	0.34[42]	0.00556[43]	0.61[44]
Zr-based glass matrix	1750	85[19]	0.38[19]	—	—

Table III. Measured Angles between Shear Bands and Loading Axis along with Angles between Stress Concentrations and Loading Axis for FEM Calculations Using the von Mises and Mohr–Coulomb Criteria; the Experimental and FEM Results are for Uniaxial Compression

Method	Angle
Shear band angles (experimental)	47.0 ± 2.0
Von Mises criterion (FEM)	47.7 ± 4.0
Mohr–Coulomb criterion (FEM)	46.0 ± 4.6

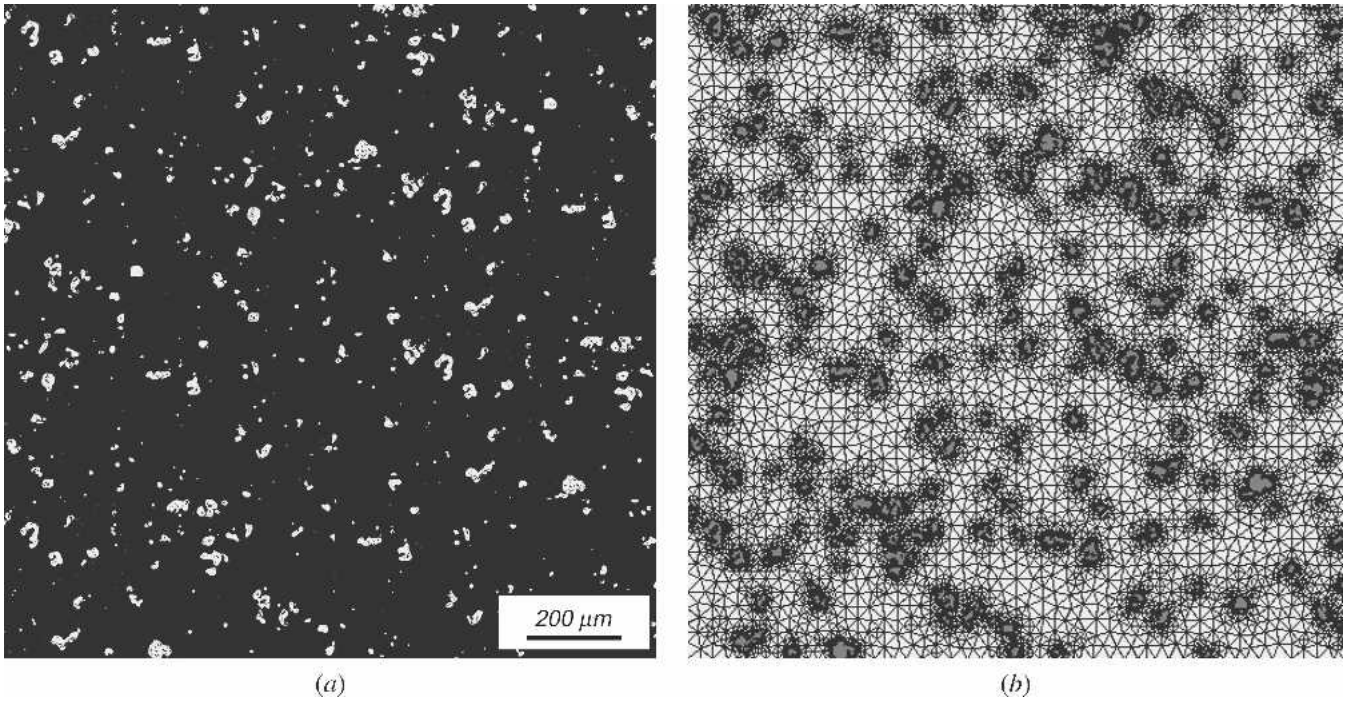

Fig. 1—(*a*) Mosaic image of the composite alloy microstructure and (*b*) the corresponding mesh used in the FEM calculations.

was calculated for all angles θ from 0 to 180 deg, where θ is the angle between the shear plane and the loading axis. The maximum calculated value of the Mohr–Coulomb stress was then assigned to its respective quadrature point along with the corresponding value of θ.

III. RESULTS AND DISCUSSION

A. *Slip Plane and Fracture Surface Angles*

The reinforcing phase in metallic-glass-matrix composites is known to serve as an initiation site for shear bands.[18,19] Figure 2 shows scanning electron microscopy (SEM) micrograph of slip steps (which represent places where shear bands intersect a free surface) for a specimen loaded to approximately 10 pct plastic strain. (For convenience, we refer to the features observed in the micrograph as ''shear bands,'' but it should be kept in mind that the shear bands themselves are too thin to be seen at the resolution of Figure 2.) Shear bands appear to initiate preferentially at the particles, which is consistent with *in-situ* X-ray diffraction studies of the strain evolution of the particles.[16] To examine how this heterogeneous initiation affects plastic flow in the composite alloys, we measured the angles between the shear bands and the compressive loading axis for the specimen shown in Figure 2. The advantage of this technique compared to measuring the fracture surface angle is that it does not assume that fracture occurs on the slip plane. For most monolithic metallic glasses loaded in an unconstrained geometry, only a limited number of shear bands develop prior to failure, making it difficult to measure the slip plane angle directly.

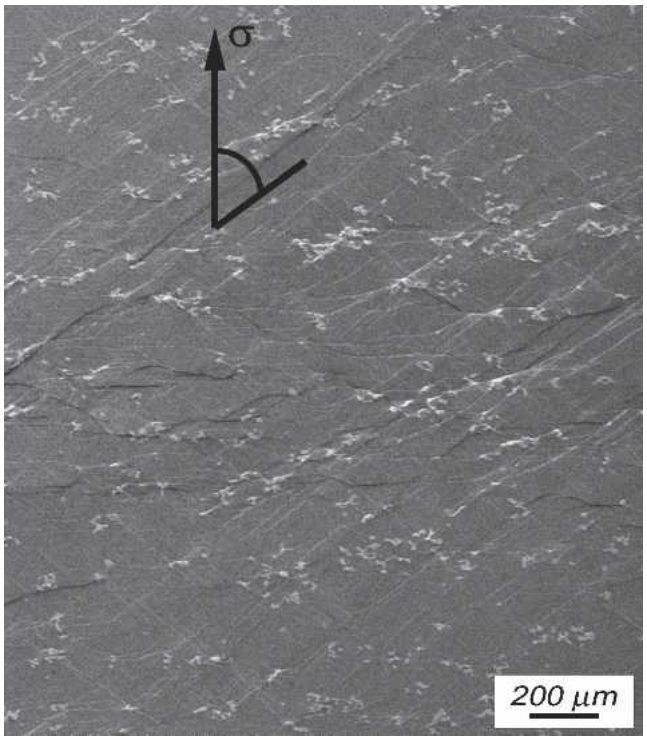

Fig. 2—Secondary SEM micrograph of shear bands initiated at the particles for sample loaded to ~10 pct plastic strain. The angle between a slip step and the loading axis is denoted.

Thus, the fracture surface angle is often reported as the slip plane angle, thereby making the implicit assumption that the yield criterion and fracture criterion are the same. Unlike monolithic metallic glasses, metallic-glass-matrix composites form multiple shear bands prior to failure, allowing for direct measurement of the slip plane angle(s). In Figure 2, slip steps with both light and dark contrast may be seen. The majority of the steps are light-colored and appear to emanate from the particles. In addition, there are a few slip steps with dark contrast, apparently because the slip offset is larger than for the steps with lighter contrast. For both cases, examples can be seen of steps at ~45 and ~90 deg to the loading axis, representing two orthogonal views with respect to the direction of shear band propagation. Finally, a few steps can be observed in which the angle is neither ~45 nor ~90 deg, or in which the angle changes along the step. For consistency of measurement, only the steps at angles of ~45 deg were used for measurements of shear band angles. The average angle between the shear bands and the loading axis was determined by measuring the angle between intersecting slip steps (under the assumption that the shear band angles are symmetric about the loading direction). As a check, the angle between individual shear bands and the loading axis was also measured. From the micrograph in Figure 2, the angle between the loading axis and the shear bands was measured for approximately 40 shear bands. In the present case, we measure an average slip plane angle of 47 $\pm$ 2 deg, somewhat larger than the fracture surface angle value of ~42 deg typically reported for single-phase metallic glasses.[3,4,20–24] It should be noted that the measured shear band angles are not necessarily representative of the slip planes at the macroscopic yield point. Instead, they represent the shear band angles where the matrix has locally yielded near the particles.

To explore the reason for the difference between the composites and single-phase glasses, we examined the stress concentrations in the amorphous matrix using FEM. For the von Mises criterion, we assume that yielding occurs when the von Mises effective stress reaches the uniaxial yield stress of the matrix, taken to be 1750 MPa. For the Mohr–Coulomb criterion, yielding occurs when the stress reaches the yield stress in pure shear, taken to be 875 MPa. Contour plots of the matrix stress calculated using the von Mises and Mohr–Coulomb criteria are shown in Figure 3. The contour plots, which have been normalized to the yield stress for the two criteria, show bands of concentrated stress localized near the particles. Since the FEM model does not account for shear band initiation and propagation, the bands observed in Figure 3 do not necessarily represent shear bands, but rather regions where shear bands might be initiated. The average angle between the stress concentration bands and the loading axis was determined as described previously. For each yield criterion, approximately 25 to 30 stress concentration bands were used. Since the stress concentrations do not necessarily represent shear bands, the selection of what constitutes a stress concentration band is somewhat subjective. For example, the contour map for the von Mises criterion shows stress concentrations between particles that are more or less parallel or perpendicular to the loading axis. The FEM of single particle systems has shown in these cases that the stress concentration does not extend far into the matrix (less than one particle diameter),

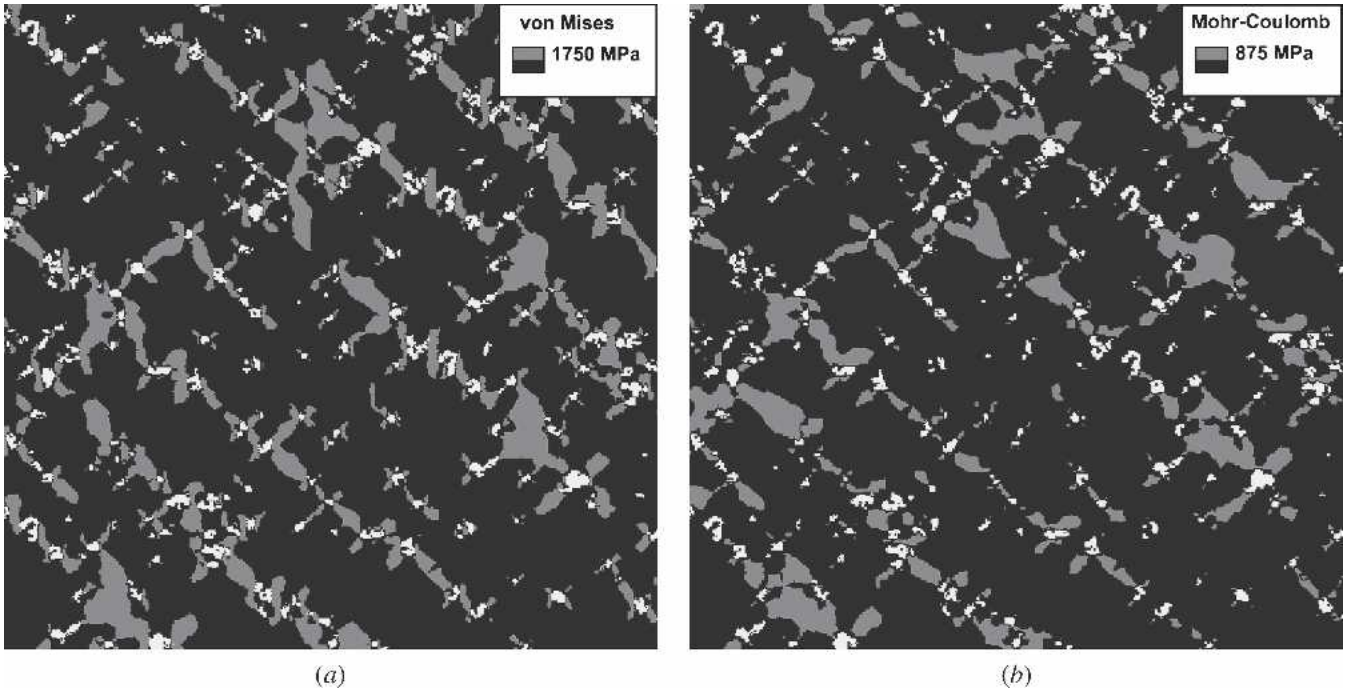

Fig. 3—Contour maps of stresses in the glass matrix calculated using the (*a*) von Mises and (*b*) Mohr–Coulomb criterion. The shaded regions correspond to the regions in the matrix where the calculated stress exceeds the materials yield stress.

and thus we do not consider them here.[16] The average angle between the stress concentration bands and the loading axis calculated based on the von Mises criterion is 48 ± 4 deg, while that based on the Mohr–Coulomb criterion is 46 ± 5 deg (Table III). Both of these are consistent with the measured value (47 ± 2 deg). In both the measurement and the models, the range of values is a reflection of the underlying inhomogeneity of the stress state of the matrix. This suggests that a prediction of shear band angles in the composite is more a function of the microstructure, which affects the stress distribution, than of the specific yield criterion chosen.

It is interesting that the average slip plane angle from both the experiments and the models is greater than 45 deg. For an isotropic sample, the plane of maximum shear for the von Mises criterion is oriented at 45 deg to the loading axis. However, the stress concentration around the particles causes the plane of maximum shear to deviate from 45 deg for the von Mises criterion. The stress state around the particles also affects the normal stress on the shear plane, and, as a result, affects the angle of the shear plane relative to the loading axis for the Mohr–Coulomb criterion as well. The effects of the particles on the angle of the plane of maximum shear stress for the Mohr–Coulomb criterion are illustrated in Figure 4. For the chosen value of $\alpha = 0.112$, the angle between the loading axis and the plane of maximum shear is 41.8 deg for an isotropic material. In Figure 4, the angle of maximum stress is indeed between 40 to 43 deg for the regions of the matrix sufficiently far removed from the particles. However, near the particles, the angle deviates from this range, and there is a significant fraction (~15 pct) of the matrix near the particles in which the maximum stress corresponds to a slip plane angle greater than 43 deg. There is also a smaller fraction of the matrix near the particles, where the maximum stress angles are less than 40 deg. This illustrates that even though the concentration of particles is low (~4 pct), it has a significant effect on the shear band angles because a majority of shear bands are initiated at the particles.

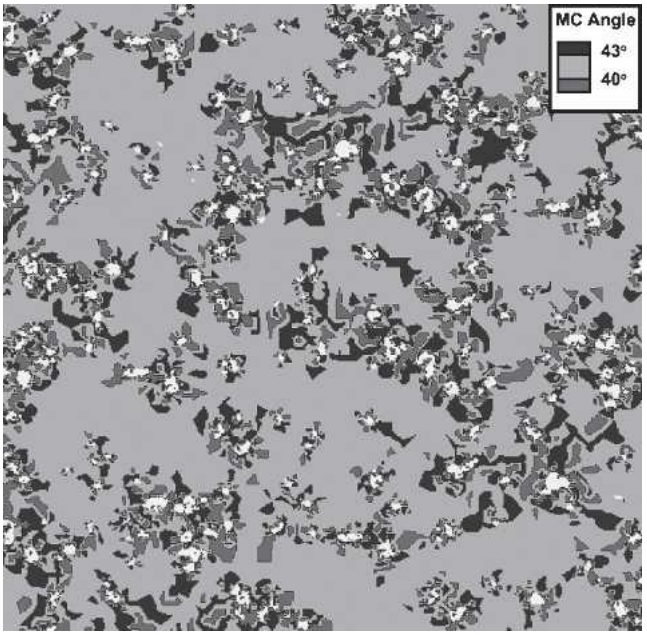

Fig. 4—Contour map of angle between slip plane and loading axis calculated using the Mohr–Coulomb criterion. The angles correspond to the maximum calculated Mohr–Coulomb stress.

Our observations call into question the validity of the assumption that the fracture angle is representative of the

shear band angle for this metallic-glass-matrix composite. To investigate this, we measured the angle between the fracture surface and the loading axis for specimens loaded at different strain rates (Figure 5(a)). For the samples loaded in uniaxial compression at strain rates of 10^{-4} and 10^{-3} s^{-1}, the fracture angles are less than 40 deg. However, for these lower strain rates, significant bending occurs along the gage length prior to failure (Reference 14), making it difficult to measure the fracture surface angle accurately. For strain rates above 10^{-3} s^{-1}, less bending occurs (Figure 5(b)), making the measured angles between the fracture surface and the compressive loading axis more accurate. For samples loaded at strain rates of 10^{-2} and 10^{-1} s^{-1}, the average fracture surface angles are 41.1 and 41.5 deg, respectively, which are consistent with the reported fracture angles for monolithic metallic glasses. Similarly, the fracture angle for samples tested in quasi-static uniaxial tension, 54.6 deg, is also consistent with the reported angles for monolithic glasses.[3,4,25,26]

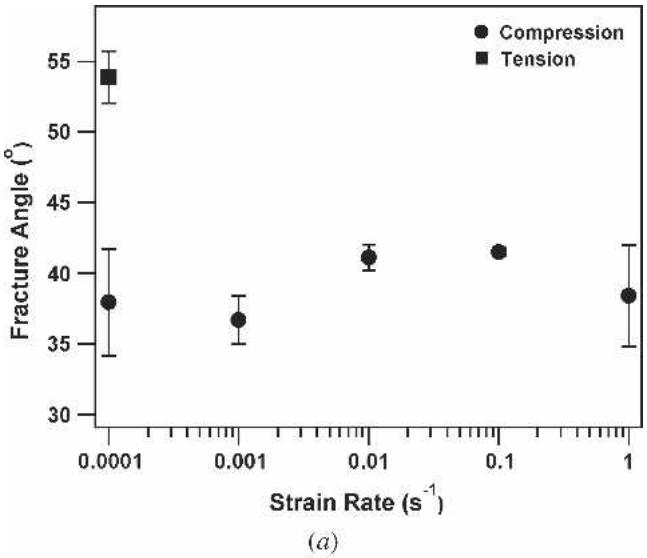

(*a*)

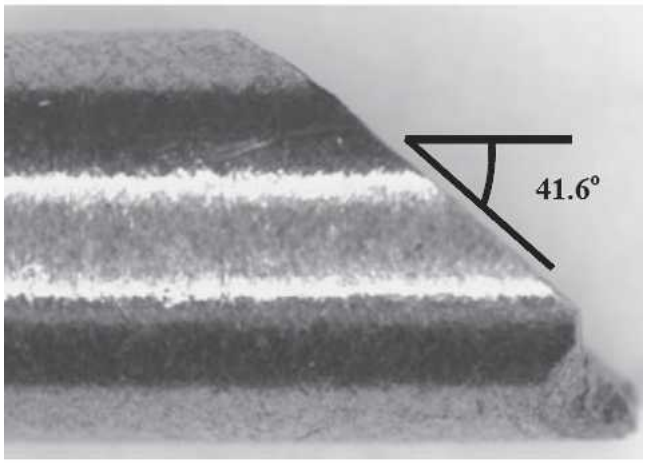

(*b*)

Fig. 5—(*a*) Angle between fracture surface and loading axis as a function of strain rate for samples loaded in uniaxial compression. (*b*) Optical micrograph of sample loaded in uniaxial compression at 10^{-2} s^{-1}. The angle between the fracture surface and the loading axis is denoted.

The fact that the slip plane angles we observe for quasi-static compression (47 ± 2 deg) are different from the fracture surface angles (~41 deg) clearly indicates that these two measurements are not equivalent for our composite materials. The stress concentrations around the particles described previously cause local yielding of the matrix, but the local stress state causes the slip plane angles to differ from what would be predicted based on the macroscopic stress state. We note that the thickness of a shear band (20 to 100 nm) is much smaller than the size of the particles,[27,28] suggesting that variations in the local stress state on the much larger scale of the particles (~50 to 100 μm) can have a significant effect on the propagation direction of a shear band. In contrast, once adiabatic softening leading to fracture sets in, the characteristic scale of the shear bands becomes much larger (~50 μm);[29] in this state, the shear band (or crack front) propagation is not as strongly influenced by local variations in stress state.

It is important to keep in mind that although the volume faction of particles is quite low (~4 pct), the inhomogeneous stress distribution that results has a measurable effect on the plastic response in terms of both yield stress and shear band orientation relative to monolithic metallic glasses of similar composition. The fracture plane angle, however, is the same for both single-phase and composite specimens. This observation suggests that once fast fracture has been initiated, the response of the material is dominated by the amorphous matrix. In this sense, the fracture behavior appears to be similar to that of a single-phase glass, although we note that no fracture toughness measurements have been made under controlled fracture conditions.

B. *Tension/Compression Asymmetry of Yield Stress*

The effects of the Ta particles on the yield criterion can also be seen by comparing the yield stresses for compressive and tensile loading. The yield stresses (calculated by the 0.2 pct offset method) for quasi-static uniaxial compression and tension are 1730 ± 10 and 1720 ± 10 MPa, respectively.[14] (It should be noted that these are engineering stresses; taking into account the Poisson effect, the true yield stresses would be approximately equal.) This is different from the behavior of monolithic metallic glasses in which the compressive yield stress has been reported to be higher than the tensile yield stress,[2,3,26,30] although not all authors are in agreement on this point[4] (Table I). Similarly, the compressive yield stress has been reported to be larger than the tensile yield stress in two-phase materials consisting of a ductile dendritic phase in a metallic-glass matrix.[11,12]

C. *Strain Rate Dependence of Yield Stress and Fracture Stress*

To further examine the deformation behavior of the composite alloys, we examined the behavior of specimens loaded in uniaxial compression over a wide range of strain rates (Figure 6). At strain rates of 10^{0} s^{-1} and below, the composites show a clear yield stress. Under dynamic loading, fracture occurs without measurable plastic deformation, so in this range we report the maximum stress, which occurs at fracture.

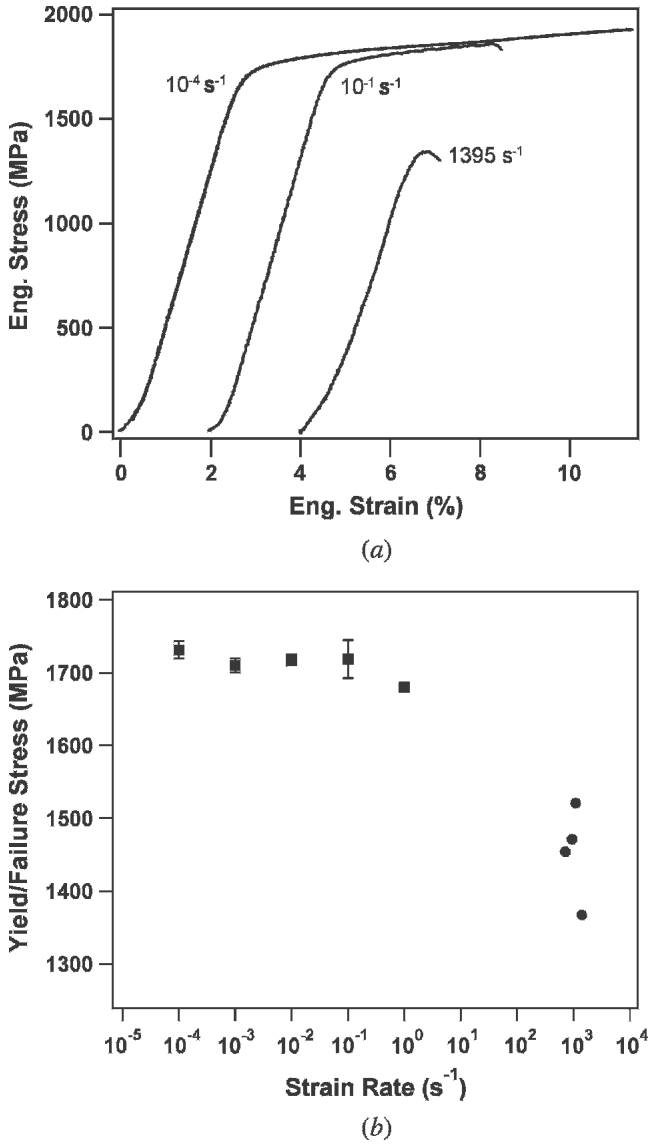

Fig. 6—(*a*) Stress-strain curves for samples loaded in uniaxial compression at different strain rates. (*b*) Yield stress (squares) and failure stress (circles) as a function of strain rate for samples loaded in uniaxial compression.

The composite yield stress does not show significant strain rate dependence for strain rates up to 10^{-1} s^{-1}, which is consistent with observations on single-phase metallic glasses.[23,26,31,32] The samples tested at 10^{0} s^{-1} show a small decrease in their yield stress compared to the lower strain rates. Sergueeva and co-workers[33] have reported a similar drop in the yield stress for a Zr-based metallic glass alloy at a strain rate of 10^{-2} s^{-1}. For the samples tested under dynamic loading conditions, the fracture stress is significantly lower than the yield stresses observed at lower rates. The decrease in the failure stress for the samples tested under dynamic compression is also characteristic of monolithic glasses.[29,31,34] Thus, the volume fraction of Ta particles is not large enough to affect the strain-rate dependence of the composite alloys. It is likely that, once a shear band is initiated at these high rates, thermal effects quickly take over, and it is the behavior of the matrix that determines the overall response of the material. This behavior is in contrast to that of composites with larger volume fractions of particles, in which the yield stress of the composite increases with increasing strain rate.[29]

IV. CONCLUSIONS

We have examined the plastic deformation and fracture behavior of metallic-glass-matrix composites containing a small volume fraction (~4 pct) of ductile second-phase particles. Experimental measurements of the average angle between the shear bands and the loading axis for uniaxial compression agree well with the FEM of yielding in the composites calculated using either the von Mises or the Mohr–Coulomb criterion, but are different from the slip plane angle for single-phase glasses. Also, we do not observe an asymmetry between the yield stress in uniaxial tension and compression. On the other hand, the strain-rate dependence of the composites is similar to that of single-phase glasses for dynamic loading, and the fracture surface angles in both tension and compression are similar to those observed for single-phase glasses.

Our results highlight the importance of a clear delineation between plastic flow behavior and fracture behavior of metallic-glass-matrix composites. In single-phase metallic glasses, it is commonly assumed that the yield stress is equivalent to the flow stress and the fracture stress, and that the slip plane angle (as it relates to yield criteria) is equivalent to the fracture surface angle. However, plastic deformation and fracture are not the same (although they are related in these materials), and there is no fundamental reason to expect that these quantities should be equivalent. In the case of metallic-glass-matrix composites with small volume fractions of particles, the distinction becomes clearer because localized yielding events are initiated by the particles while the fracture behavior is still governed by the properties of the amorphous matrix.

ACKNOWLEDGMENTS

This work was performed under the auspices of the Center for Advanced Metallic and Ceramic Systems (CAMCS), Johns Hopkins University. This research was sponsored by the Army Research Laboratory (ARMAC-RTP) and was accomplished under ARMAC-RTP Cooperative Agreement No. DAAD19-01-2-0003.

REFERENCES

1. H. Kimura and T. Masumoto: *Acta Metall.*, 1980, vol. 28, pp. 1663-75.
2. P.E. Donovan: *Acta Metall.*, 1989, vol. 37, pp. 445-56.
3. Z.F. Zhang, J. Eckert, and L. Schultz: *Acta Mater.*, 2003, vol. 51, pp. 1167-79.
4. J.J. Lewandowski and P. Lowhaphandu: *Philos. Mag. A*, 2002, vol. 82, pp. 3427-41.
5. R. Vaidyanathan, M. Dao, G. Ravichandran, and S. Suresh: *Acta Mater.*, 2001, vol. 49, pp. 3781-89.
6. C.A. Schuh and T.G. Nieh: *J. Mater. Res.*, 2004, vol. 19, pp. 46-57.
7. C.A. Schuh and A.C. Lund: *Nat. Mater.*, 2003, vol. 2, pp. 449-52.
8. A.C. Lund and C.A. Schuh: *Acta Mater.*, 2003, vol. 51, pp. 5399-41.
9. A.C. Lund and C.A. Schuh: *Intermetallics*, 2004, vol. 12, pp. 1159-65.
10. Z.F. Zhang and J. Eckert: *Phys. Rev. Lett.*, 2005, vol. 94, p. 094301.
11. F. Szuecs, C.P. Kim, and W.L. Johnson: *Acta Mater.*, 2001, vol. 49, pp. 1507-13.

12. M.L. Lee, Y. Li, and C.A. Schuh: *Acta Mater.*, 2004, vol. 52, pp. 4121-31.
13. J.C. Lee, Y.C. Kim, J.P. Ahn, and H.S. Kim: *Acta Mater.*, 2005, vol. 53, pp. 129-39.
14. C. Fan, R.T. Ott, and T.C. Hufnagel: *Appl. Phys. Lett.*, 2002, vol. 81, pp. 1020-22.
15. R.S. Coates and K.T. Ramesh: *Mater. Sci. Eng., A*, 1991, vol. 145, pp. 159-66.
16. R.T. Ott, F. Sansoz, J.F. Molinari, J. Almer, K.T. Ramesh, and T.C. Hufnagel: *Acta Mater.*, 2005, vol. 53, pp. 1883-93.
17. ppm2oof, software, http://www.ctcms.nist.gov/oof.
18. R.D. Conner, R.B. Dandliker, and W.L. Johnson: *Acta Mater.*, 1998, vol. 46, pp. 6089.
19. H. Choi-Yim, R.D. Conner, F. Szuecs, and W.L. Johnson: *Acta Mater.*, 2002, vol. 50, pp. 2737-45.
20. G. He, J. Lu, Z. Bian, D. Chen, G. Chen, G. Tu, and C. Chen: *Mater. Trans., JIM*, 2001, vol. 42, pp. 356-64.
21. W.J. Wright, R. Saha, and W.D. Nix: *Mater. Trans., JIM*, 2001, vol. 42, pp. 642-49.
22. P. Wesseling, P. Lowhaphandu, and J.J. Lewandowski: *Mater. Res. Soc. Proc.*, 2003.
23. T. Mukai, T.G. Nieh, Y. Kawamura, A. Inoue, and K. Higashi: *Scripta Mater.*, 2002, vol. 46, pp. 43-47.
24. Z.F. Zhang, J. Eckert, and L. Schultz: *J. Mater. Res.*, 2003, vol. 18, pp. 456-65.
25. C.T. Liu, L. Heatherly, D.S. Easton, C.A. Carmichael, J.H. Schneibel, C.H. Chen, J.L. Wright, M.H. Yoo, J.A. Horton, and A. Inoue: *Metall. Mater. Trans. A*, 1998, vol. 29, pp. 1811-20.
26. T. Mukai, T.G. Nieh, Y. Kawamura, A. Inoue, and K. Higashi: *Intermetallics*, 2002, vol. 10, pp. 1071-77.
27. P.E. Donovan and W.M. Stobbs: *Acta Metall.*, 1981, vol. 29, pp. 1419-36.
28. J. Li, F. Spaepen, and T.C. Hufnagel: *Philos. Mag. A*, 2002, vol. 82, pp. 2623-30.
29. T. Jiao, L.J. Kecskes, T.C. Hufnagel, and K.T. Ramesh: *Metall. Mater. Trans. A*, 2004, vol. 35, pp. 3439-44.
30. T. Erturk and A.S. Argon: *J. Mater. Sci.*, 1987, vol. 22, pp. 1365-73.
31. T.C. Hufnagel, T. Jiao, Y. Li, L.Q. Xing, and K.T. Ramesh: *J. Mater. Res.*, 2002, vol. 17, pp. 1441-45.
32. H.A. Bruck, A.J. Rosakis, and W.L. Johnson: *J. Mater. Res.*, 1996, vol. 11, pp. 503-11.
33. A.V. Sergueeva, N.A. Mara, J.D. Kuntz, E.J. Lavernia, and K.A. Mukherjee: *Philos. Mag.*, 2005, vol. 83, pp. 2671-87.
34. H. Li, G. Subhash, X.-L. Gao, L.J. Kecskes, and R.J. Dowding: *Scripta Mater.*, 2003, vol. 49, pp. 1087-92.
35. T. Masumoto and R. Maddin: *Acta Metall.*, 1971, vol. 19, pp. 725-41.
36. H.J. Leamy, H.S. Chen, and T.T. Wang: *Metall. Trans.*, 1972, vol. 3, pp. 699-708.
37. T. Murata, T. Masumoto, and M. Sakai: *Rapidly Quenched Metals II,* The Metals Society, London, 1978. pp. 401-04.
38. S. Takayama: *Scripta Metall.*, 1979, vol. 13, pp. 463-67.
39. H. Kimura and T. Masumoto: *Amorphous Metallic Alloys*, Butterworths and Co., London, 1983. pp. 187-230.
40. P.E. Donovan: *Mater. Sci. Eng.*, 1988, vol. 98, pp. 487-90.
41. C.A. Pampillo and D.E. Polk: *Acta Metall.*, 1974, vol. 22, pp. 741-49.
42. *Handbook of Elastic Properties of Solids: Liquids, and Gases*, Academic Press, San Diego, CA, 2001.
43. S.R. Chen and G.T. Gray III: *Metall. Mater. Trans. A,* 1996, vol. 27, pp. 2994-3006.
44. A.S. Khan and R. Liang: *Int. J. Plast.*, 1999, vol. 15, pp. 1089-109.